Dalton Transactions

Observation of Current Rectification by the New Bimetallic Iron(III) Hydrophobe [FeIII2(LN4O6)] on Au|LB-Molecule|Au Devices

Journal:	*Dalton Transactions*
Manuscript ID	DT-ART-08-2018-003158.R1
Article Type:	Paper
Date Submitted by the Author:	04-Sep-2018

Complete List of Authors:	Weeraratne, Aldora ; Wayne State University, Chemistry Baydoun, Habib; Wayne State University, Chemistry Shakya, Rajendra; Broward College , Physical Science Niklas, Jens; Argonne National Laboratory, Chemical Sciences & Engineering Xie, Lingxiao; Wayne State University, Chemical Engineering Mao, Guangzhao; Wayne State University, Chemical Engineering Stoian, Sebastian; University of Idaho, Chemistry Poluektov, Oleg; Argonne National Laboratory, Chemical Sciences and Engineering Division Verani, Claudio; Wayne State University, Chemistry

Journal Name

ARTICLE

Observation of Current Rectification by the New Bimetallic Iron(III) Hydrophobe $[Fe^{III}_2(L^{N4O6})]$ on Au|LB-Molecule|Au Devices

Received 00th January 20xx,
Accepted 00th January 20xx

DOI: 10.1039/x0xx00000x

www.rsc.org/

A. D. K. Isuri Weeraratne,[a] Habib Baydoun,[a] Rajendra Shakya,[a,†] Jens Niklas,[b] Lingxiao Xie,[c] Guangzhao Mao,[c] Sebastian A. Stoian,[d] Oleg Poluektov,[b] and Cláudio N. Verani[a,*]

Targeting the development of stimulus-responsive molecular materials with electronic functionality, we have synthesized and studied the redox and electronic properties of a new bimetallic iron hydrophobe $[Fe^{III}_2(L^{N4O6})]$ **(1)**. The new H_6L^{N4O6} ligand displays bicompartmental topology capable of accomodating two five-coordinate $^{HS}Fe^{III}$ ions bridged by tetraaminobenzene at a close distance of *ca*. 8 Å. We show that the metal-based reduction processes in **(1)** proceed sequentially, as observed for electronically coupled metal centers. This species forms a well-defined Pockels-Langmuir film at the air-water interface, with collapse pressure of 32 mN/m. Langmuir-Blodgett monolayers were deposited on gold substrates and used to investigate current-voltage (*I-V*) measurements. This unprecedented bimetallic hydrophobe $[Fe^{III}_2(L^{N4O6})]$ **(1)** shows unquestionable molecular rectification and displays a rectification ratio *RR* between 2 and 15.

Dedicated to the memory of Dr. Mary Jane Heeg (1952-2018) for her contributions to X-ray crystallography.

Introduction

Solid state rectifier diodes, similar to check valves for liquids, allow unidirectional flow of current in electronic circuitry. Aviram & Ratner proposed that this process may be scaled further down to molecular devices based on an electrode|molecule|electrode architecture[1] where suitable molecules are expected to display distinct donor (D) and acceptor (A) moieties that show moderate coupling *via* a bridge (b). These molecules usually display a neutral ground state [D-b-A] and a charge-separated $[D^+\text{-b-}A^-]$ excited state of higher but accessible energy.[1,2,3] Additionally some zwitterionic rectifiers display a $[D^+\text{-b-}A^-]$ ground state.[2b,3] Rectification takes place if the respective energies of the frontier highest occupied and lowest unoccupied molecular orbitals (MOs) are energetically close to the Fermi levels of the electrodes.[4] Traditionally, these systems have been synthesized using purely organic molecules.[5-11] Nonetheless, rectifiers based on coordination complexes, particularly with ferrocene, porphyrin and terpyridine moieties, are also attracting interest.[12-20] Recent efforts spearheaded by our group have expanded considerably the vocabulary of molecular rectification by using arguments of ligand field theory to obtain high-spin $^{HS}3d^5$ iron(III)-containing phenolate-rich surfactants of low symmetry described as $[Fe^{III}(L^{N2O3})]$ (**1**).[21,4] When the rectifying activity of such species was compared to that of equivalent $[Cu^{II}(L^{N2O2})Cl]$ surfactants with a $3d^9$ configuration where the $3(d_{x2-y2})^1$ MO shows inaccessible energy, an insulating behavior was observed. This enabled us to conclude that rectification proceeds *via* the singly-occupied molecular orbitals (SOMOs) of the metal *via* an asymmetric mechanism.[22] Therefore, the spatial and energetic modulation of the SOMO orbitals is an essential step towards the design of diode-like molecules with rectifying properties.[4] Because our rectifiers display five-coordination, rectification must be attained with either low molecular symmetry or local orbital distortion provided by the different N and O donor sets.

Building on our interest in the modulation of the frontier orbitals, we hypothesize that the use of a bimetallic $[Fe^{III}]_2$ system may allow for inference on the role played by low molecular symmetry and orbital distortion. The overall molecule displays a low idealized C_{2v} symmetry where both metal ions show comparable orbital distortion. Furthermore, such a molecule could lead to some degree of electronic coupling of the metal centers and therefore facilitate SOMO-based electron transfer expected to enhance the rectification behavior of our assembly. As such, we synthesized the new homobimetalic iron(III) complex $[Fe^{III}_2(L^{N4O6})]$ (**1**) which is based on the new bicompartmental ligand H_6L^{N4O6} in which two N_2O_3 binding cavities are connected *via* a tetraamino bridge. Because of the quasi-planar nature of the complex and the presence of eighteen tertiary butyl groups, this species

[a] Department of Chemistry, Wayne State University, Detroit, MI 48202, USA. E-mail: cnverani@chem.wayne.edu.
[b] Chemical Sciences & Engineering Division, Argonne National Laboratory, Lemont, IL 60439, USA.
[c] Department of Chemical Engineering & Materials Science, Wayne State University, Detroit, MI 48202, USA.
[d] Department of Chemistry, University of Idaho, Moscow, ID 83844, USA.
† Current address: Broward College, Fort Lauderdale, FL 33301, USA.
Electronic Supplementary Information (ESI) available: Spectrometric, structural, spectroscopic, redox, and I/V data. See DOI: 10.1039/x0xx00000x

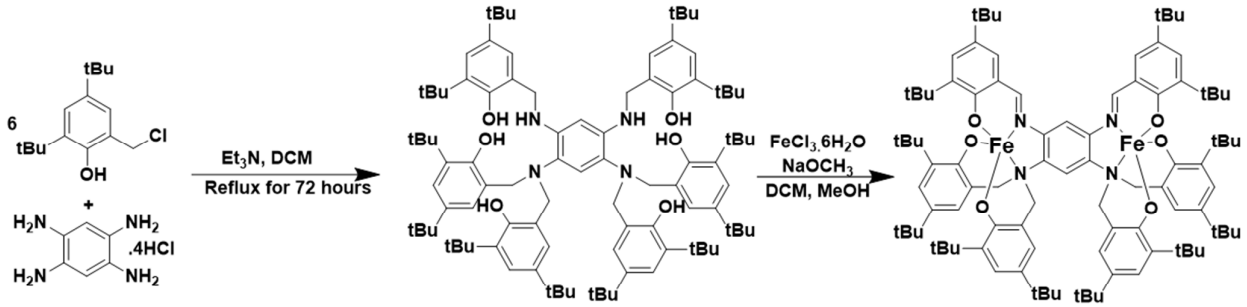

Scheme 1: Synthesis of H_6L^{N2O6} and $[Fe^{III}_2(L^{N4O6})]$ (**1**).

behaves as a hydrophobe able to form Langmuir-Blodgett films needed for device fabrication. The results follow.

Results and Discussion

Synthesis and structural characterizations

The new ligand H_6L^{N4O6} was synthesized by the nucleophilic substitution reaction of 1,2,4,5-benzene tetramine tetrahydrochloride with six equivalents of 2,4-di-tert-butyl-6-(chloro methyl)phenol in presence of excess triethylamine (**Scheme 1**).

The metal complex $[Fe^{III}_2(L^{N4O6})]$ (**1**) was prepared by the treatment of H_6L^{N4O6} with $FeCl_3.6H_2O$ in methanol, using $NaOCH_3$ as base to deprotonate the phenol groups into coordinating phenolates. The Fourier-Transform infrared (FTIR) spectrum of the complex showed a distinct C=N stretch at 1579 cm^{-1}. Along with the absence of N-H peaks, this indicates that the two secondary amine groups were oxidized to the imine form during the complexation process. This behavior has been observed during complexation in similar tris phenolate ligand environments under aerobic conditions and was studied in detail elsewhere.[23,24] The high-resolution mass spectrum of the compound showed a peak cluster at 1550.8939 (**Figure S1a**), which corresponds to $[Fe^{III}_2(L^{N4O6}) + H^+]^+$. The elemental analysis supported the proposed structural assignment.

X-ray quality crystals were grown from the parent solution *via* slow evaporation of dichloromethane (DCM) and methanol. The unit cell contains a single molecule of (**1**), in which two binding cavities are separated by a tetraaminobenzene bridge that imposes an Fe-Fe distance of 8.26 Å. Moreover, short N(2)-C(86) and N(3)-C(9) bond lengths confirm the complete conversion of the ligand amines into imines in excellent agreement with the FTIR spectrum. Interestingly, the two imine nitrogen atoms are *cis* to one another with respect to the bridge. Finally, as desired for rectification, the iron centers are in a five-coordinate geometry. Each of those ions display a τ value[25] of 0.69 and 0.74 associated with a distorted trigonal bipyramidal geometry.

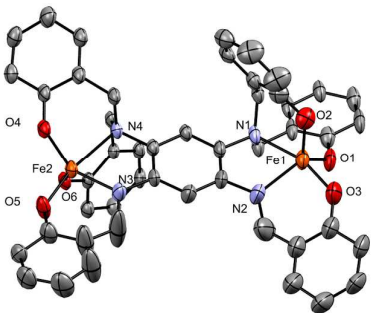

Figure 1: The crystal structure of $[Fe^{III}_2(L^{N4O6})]$ (**1**) (CCDC 1842912) Hydrogen atoms and t-butyl groups have been removed for clarity, ellipsoids are drawn at 50 % probability. Selected bond lengths for Fe2L: Fe(1)-O(1) = 1.903(4), Fe(1)-O(2) = 1.828(4), Fe(1)-O(3) = 1.862(4), Fe(1)-N(1) = 2.220(4), Fe(1)-N(2) = 2.112(5), Fe(2)-O(4) = 1.885(3), Fe(2)-O(5) = 1.860(3), Fe(2)-O(6) = 1.836(3), Fe(2)-N(3) = 2.137(4), Fe(2)-N(4) = 2.234(3), N(2)-C(86) = 1.284(9), N(3)-C(9) = 1.331(10).

Redox and electronic behavior

Cyclic voltammetry of $[Fe^{III}_2(L^{N4O6})]$ (**1**) revealed rich electrochemical response consisting of three two-electron oxidation processes at 0.57 $V_{Fc+/Fc}$ (ΔE_p = 0.12 V, $|I_{pa}/I_{pc}|$ = 2.0), 0.79 $V_{Fc+/Fc}$ (ΔE_p = 0.17 V, $|I_{pa}/I_{pc}|$ = 0.142), and 1.17 (E_{Pa}) $V_{Fc+/Fc}$, attributed to conversions from phenolate to phenoxyl radical. This behavior is expected for environments with structurally equivalent moieties. Furthermore, two one-electron reduction processes observed at -1.27 $V_{Fc+/Fc}$ (ΔE_p = 0.11 V, $|I_{pa}/I_{pc}|$ = 0.68) and -1.44 $V_{Fc+/Fc}$ (ΔE_p = 0.11 V, $|I_{pa}/I_{pc}|$ = 1.01) were attributed to the sequential reduction $[Fe^{III}Fe^{III}] \rightarrow$

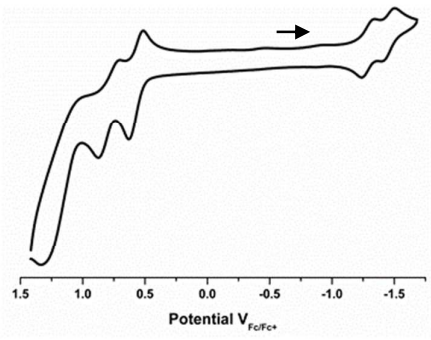

Figure 2: The CV of $[Fe^{III}_2(L^{N4O6})]$ (1mM) in DCM. $TBAPF_6$ supporting electrolyte, glassy carbon (WE), Ag/AgCl (RE), Pt wire (AE). Ferrocene is used as an internal standard. Resting potential -0.5 $V_{Fc+/Fc}$.

$[Fe^{III}Fe^{II}] \rightarrow [Fe^{II}Fe^{II}]$, or (**1**) to (**1'**) to (**1"**) (**Figure 2**).

We considered the possibility of ligand-centered reductions described as $[Fe^{III}Fe^{III}L] \rightarrow [Fe^{III}Fe^{II}L] \rightarrow [Fe^{III}Fe^{II}L\bullet]$, or (**1**) to (**1'**) to (**1'•**). However, while this is the case for quinonoid chloranilates[26] and tetraazalenes,[27] the tetrasubstituted benzene ligands pioneered by Collins[28] and Journaux[29] only show radical formation at considerably lower negative potentials. Because the ligand H_6L^1 is structurally similar to tetrasubstituted benzene ligands, and because ligand reduction in the similar $[Ga^{III}{}_2(L^{N4O6})]$ (**2**) appears at 1.79 $V_{Fc+/Fc}$ (see **Figures S2, S3, S4**) we consider both reductions as metal-based. The EPR data, discussed later, support this argument. Therefore the sequential $[Fe^{III}Fe^{III}] \rightarrow [Fe^{II}Fe^{II}]$ reduction could suggest some degree of coexistence of intermediate mixed valence $[Fe^{III}Fe^{II}]$ species[30] with weak electronic coupling between the two centers. This is likely due to variations of the local τ value associated with dissimilar ligand fields when in solution. This weak coupling can be measured using the separation of 160 mV (**Figure S5**) between the metal-centered redox processes in terms of comproportionation constant K_c given in **Equation 1**.[31-33]

$K_c = \{[Fe^{III} - Fe^{II}]^2/[Fe^{III} - Fe^{III}][Fe^{II} - Fe^{II}]\} = \exp^{\Delta E1/2F\ /RT}$ (**Equation 1**)

Where $\Delta E_{1/2}$ is the separation between the first and second waves, as measured in millivolts, *F* is the Faraday constant, *R* is the universal gas constant and *T* is the temperature in Kelvin. This leads to $K_c \approx 10^3$, expected in a Robin-Day class II complex. Hence, the two metal centers are weakly coupled allowing the feasibility of an $[Fe^{III}Fe^{II}] \leftrightarrow [Fe^{II}Fe^{III}]$ equilibrium. This coupling suggests that intramolecular electron transfer relevant for rectification can take place, and is in good agreement with a weak antiferromagnetic coupling of $J \approx 3$ cm^{-1} experimentally observed by SQUID magnetization and EPR methods in a heterodinuclear $[Cu^{II}Fe^{III}]$ species.[24] In order to confirm the strength of the magnetic interactions involving the two $^{HS}3d^5$ iron(III) ions present in **(1)** we have performed a series of broken symmetry DFT calculations. The exchange coupling constant (in the $\hat{\mathbf{H}} = \boldsymbol{J}\hat{\mathbf{S}}_1 \cdot \hat{\mathbf{S}}_2$ notation) was obtained using the B3LYP/6-311G functional/basis set combination for both the unabridged X-ray structure and for a simplified and geometry-optimized computational model (see **Table T4**). As expected, these calculations predicted a weak antiferromagnetic coupling characterized by $J = 0.83$ cm^{-1} for the geometry optimized X-ray structure. A comparable value of 0.65 cm^{-1} was found for the original and non-optimized structure (**Table T5**). To assess the validity of these calculations we have calculated the exchange coupling constant for the $[Cu^{II}Fe^{III}]$ heterodinuclear complex, previously experimentally characterized. In this case we obtained $J = 2.01$ cm^{-1} (1.78 for the non optimized structure), thus in good agreement with the experimental value.

The electronic spectrum of $[Fe^{III}{}_2(L^{N4O6})]$ (**1**) taken in the UV-visible region (**Figure S6**) reveals three distinct absorption bands; the first appears at 285 nm (ε = 29,700 L mol^{-1} cm^{-1}) and is associated with a π-π* intraligand charge transfer,[23] while absorption peaks at 320 nm (ε = 25,000 L mol^{-1} cm^{-1}) and 434 nm (ε = 13,600 L mol^{-1} cm^{-1}) are respectively attributed to N_{imine}-to-iron and phenolate-to-iron ligand to metal charge transfers (LMCT).[23] The latter transition is mainly attributed to in-plane and out-of-plane $p\pi_{phenolate} \rightarrow d\sigma^*_{Fe}$ and $p\pi_{phenolate} \rightarrow d\pi^*_{Fe}$ transitions.[23]

Spectroelectrochemistry of (**1**) following the first reduction process at an applied potential of -1.35 $V_{Fc+/Fc}$ revealed a featureless decrease in absorption intensity in the range of 350 to 550 nm (**Figure 3a**). This decrease in intensity is consistent with a one-electron metal-based reduction of (**1**) to a mixed valent product $[Fe^{III}Fe^{II}(L^{N4O6})]$. The formation of Fe^{II} would partially extinguish the LMCT transitions from taking place due to occupation of a low-lying metal-based SOMO thus explaining the decrease in intensity in the CT region. On the other hand, spectroelectrochemistry following the second reduction at an applied potential of -1.70 $V_{Fc+/Fc}$ revealed two consecutive processes, as shown in **Figure 3b**. The first detailed in **Figure 3c** is similar to that obtained for the one-electron reduction product (**Figure 3a**), which suggests an initial conversion from (**1**) to $[Fe^{III}Fe^{II}(L^{N4O6})]$. The second (**Figure 3d**) consists of a decrease in the absorption bands at 350 and 500 nm, as well as an increase in the absorption band at 450 nm. These changes were also accompanied by the formation of isosbestic points at 404, 484, and 630 nm. The decline in absorption at 350 and 500 nm is attributed to a decrease in the LMCT bands, while the increase at 450 is consistent with the formation of a new phenolate-to-imine intraligand CT band.[34]

Figure 4 compares the EPR data for the equivalent monometallic species $[Fe^{III}L^{N2O3}]$[35] in spectrum (**a**) with that of the bimetallic $[Fe^{III}{}_2(L^{N4O6})]$ (**1**) in spectrum (**b**). While spectrum (**a**) shows a distinctive signal around 1500 G with g = 4.3 diagnostic of a five-coordinate $^{HS}3d^5$ species in a largely anisotropic ligand field,[34] the bimetallic species is EPR silent, as indicative of antiferromagnetic coupling among the two $^{HS}3d^5$ centers with S = 5/2 – 5/2 = 0. This assignment is based on the observation and detailed study of a similar heterodinuclear

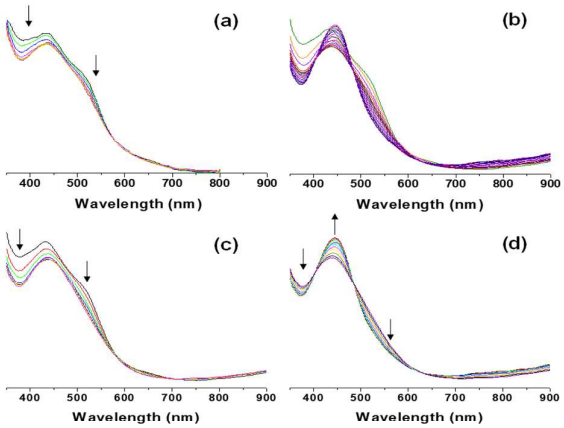

Figure 3: UV-visible absorption spectroelectrochemistry in DCM at RT following the first reduction (a), and the second reduction (b). Plots (c) and (d) show the first and second trend seen in spectrum (b). See text for details.

[$Cu^{II}Fe^{III}$] species,[24] where even couplings of very weak magnitude suffice for the signal to disappear. A weak magnetic coupling is in good agreement with the weak electronic coupling described above. A one-electron reduction of (**1**) leads to the formation of an [$Fe^{III}Fe^{II}$] species, as seen in spectrum (**c**). This species is expected to be predominantly described by an S = 1/2 signal at g ≈ 2 around 3350 G, and resulting from the antiferromagnetic coupling between $^{HS}3d^5Fe^{III}$ (S = 5/2) and $^{HS}3d^6$ Fe^{II} (S = 4/2). Indeed, this is the major component of the spectrum. Additionally, a smaller signal at g ≈ 4.3 appears to be associated with a spin 5/2 attributed to the presence of monometallated [$Fe^{III}(L^{N4O6})$]. Because this signal was not present in the EPR of (**1**), we assume that a reduction of the parent species into its [$Fe^{III}Fe^{II}$] equivalent prompts some demetallation of the more labile $3d^6$ Fe^{II} ion, as recently observed by Brand et al.[36] Attempts at both simultaneous and sequential two-electron bulk electrolysis to attain the fully reduced [$Fe^{II}Fe^{II}$] species resulted in slow and sluggish processes that ultimately led to the decomposition of (**1**).

Analysis of feasibility of rectification

Directional electron transfer, or rectification, can only take place if there is an energy match between the Fermi levels (E_F) of the gold electrode and the frontier orbitals of the rectifying molecule. The energies associated with the frontier orbitals for [$Fe^{III}{}_2(L^{N4O6})$] (**1**) can be assessed with the data provided by the electrochemical measurement of reduction and oxidation potentials. These energies can be calculated considering V_a = 4.7 eV + $E_{1/2}{}^{red}$ (vs. SCE), and V_i = 4.7 eV + 1.7$E_{1/2}{}^{ox}$ (vs. SCE), where V_a and V_i are a good approximation to the equivalent first electron affinity and first ionization energy respectively.

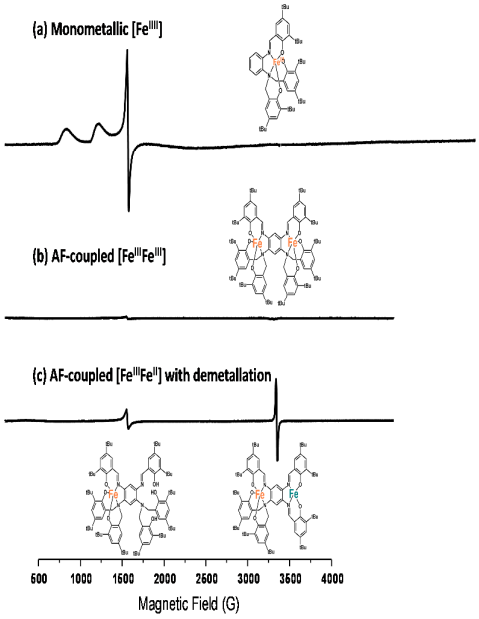

Figure 4: EPR spectra of (a) [$Fe^{III}(L^{N2O3})$], (b) [$Fe^{III}{}_2(L^{N4O6})$], and (c) [$Fe^{III}Fe^{II}(L^{N4O6})$] with some demetallation in DCM.

While gold has an E_F value of -5.1 eV below vacuum,[37, 38] the first metal-based singly occupied MO has a V_a of -3.8 eV which is 1.3 eV above the gold electrode Fermi levels. Conversely, the energy of the highest occupied MO is -6.4 eV, which is 1.3 eV below the Fermi levels of the gold electrode. The match between the Fermi and SOMO energy levels is similar to other systems where rectification has been observed experimentally[4, 21, 22a, 39] and therefore, leads us to conclude that molecular rectification will take place.

Interfacial behavior

Complementary to the necessary electronic behavior, appropriate interfacial behavior must be attained to enable the construction of devices capable of current rectification. For [$Fe^{III}{}_2(L^{N4O6})$] (**1**), some caution is needed because the system deviates from the expected amphiphilic behavior. The presence of tert-butyl-substituted phenolate groups, and the absence of well-defined polar headgroups or alkoxy chains renders a primarily hydrophobic nature.[40] Nonetheless, this hydrophobic nature, aligned with the previously discussed redox behavior, makes (**1**) a good candidate for formation of redox-responsive Langmuir-Blodgett (LB) monolayer films on solid.[41-44] Indeed, the isothermal compression curve obtained for (**1**) shown in **Figure 5** suggests that the complex can form homogenous Pockels-Langmuir (PL) films at the air/water interface. The absence of phase transitions, along with collapse at 32 mN/m are in good agreement with a constant pressure mechanism.[45] Furthermore, the collapse, as observed by Brewster angle microscopy (BAM), is marked by sporadic ridges and Newton circles attributed to multilayer granule formation from ejection of matter due to localized oscillations.[46] This behavior is similar to other flat hydrophobes investigated by our group.[40] BAM images support the

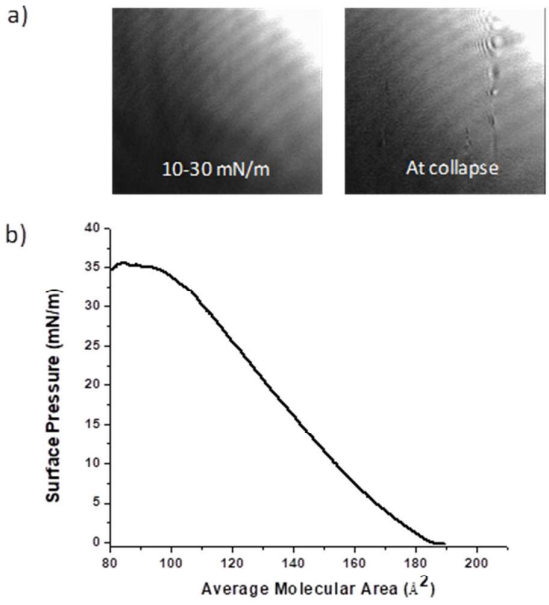

Figure 5. (a) Selected BAM images (b) Compression isotherm for [$Fe^{III}{}_2(L^{N4O6})$] (**1**).

formation of a homogenous PL film between 10 and 30 mN m^{-1}, whereas the formation of Newton rings above 30 mN m^{-1}, are indicative of collapse. The average limiting area per molecule is close to 185 $Å^2$/molecule.

The identity of the deposited hydrophobes was verified by electrospray ionization mass spectrometry (ESI-MS) and infrared reflection absorption spectrum (IRRAS). ESI-MS confirmed that the bulk $[Fe^{III}_2(L^{N4O6})]$ (**1**) prior to deposition, and that scraped off of LB films deposited as multilayers on glass substrates present the same isotopic envelopes and m/z values (**Figure S1b**). IRRAS uses s-polarized light at an angle of incidence of 40° and is compared to the IR spectrum of the bulk sample in **Figure 6**. Equivalent peak patterns were observed for both the IRRAS of the LB film and the bulk samples, showing prominent peaks due to aromatic C=C stretching and CH_3/CH_2 deformation bands at 1610-1360 cm^{-1}. A stretching vibration at 1580 cm^{-1} confirms the presence of C=N groups associated with the imine ligand, which remains intact after film deposition.[22a] Symmetric and antisymmetric stretching vibrations of CH_2 groups were observed in bulk and in the LB film between 2850 cm^{-1} to 2920 cm^{-1}. The most prominent asymmetric CH_3 vibrations in the bulk sample appear at 1955 cm^{-1} and are shifted to 1962 cm^{-1} in the LB film. Shifting of the wavenumbers is associated with a well packed film.[21,22a] In IRRAS the C-H stretching region bands are pointing downwards while fingerprint region peaks are pointing upwards. This detection of positive (upward) and negative (downward) bands is explained by means of surface selection rules: a monolayer deposited on dielectric substrates displays positive bands for vibrations with perpendicular transition dipole moment, whereas negative bands will be observed for vibrations with parallel transition dipole moments.[47,48]

Atomic force microscopy (AFM) images were taken for LB monolayers deposited on mica substrates at the four different surface pressures of 17, 20, 25 and 30 mN/m. The transfer ratio was kept near unity during the deposition of the monolayers. Films deposited at lower surface pressures show higher pinhole defects and films deposited at higher surface pressures shows higher surface aggregation, while films deposited at 25 mN/m show ordered and defect-free film formation (**Figure 7**). Therefore, films deposited around that region were selected for device fabrication. Blade-scratching[21] was used to determine the monolayer thickness of the LB films deposited on quartz substrates. One to nine layers were deposited, and films were scratched. The depth of the scratch was determined using tapping mode and a linear relationship between the thickness and the number of layers indicated the average thickness of ca. 33 to 35 Å per monolayer. The results, including AFM height images, 2D and 3D view, sectional analysis, and a plot of thickness (nm) vs. number of layers are shown in **Figure S7**. Using data from the X-ray structure, the molecule can be approximately described as a cylinder of radius r ≈ 8 Å and height h ≈ 17 Å, thus yielding a sectional area

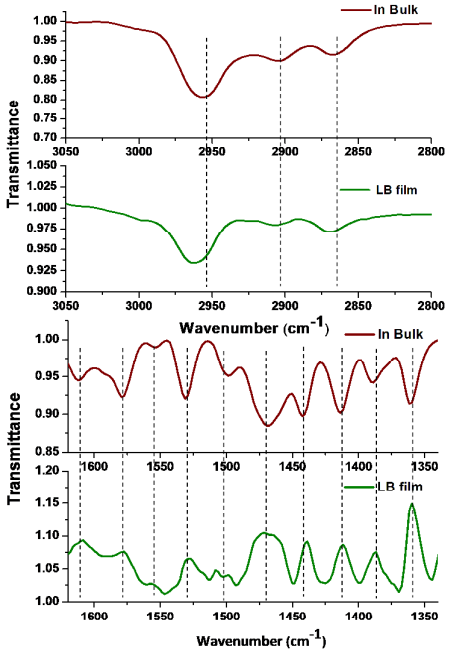

Figure 6. Comparison of the IR spectrum of $[Fe^{III}_2(L^{N4O6})]$ (**1**) in KBr and IRRAS spectrum of 61-layer LB film.

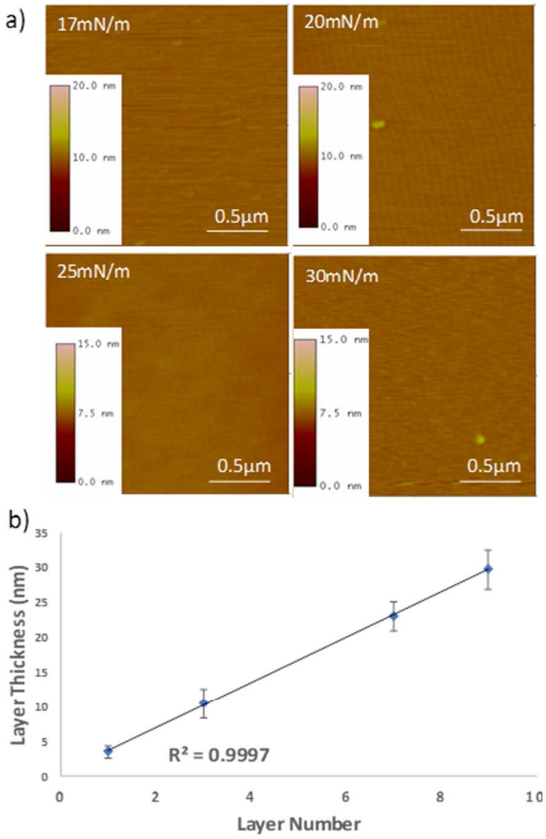

Figure 7. (a) AFM images of monolayers of $[Fe^{III}_2(L^{N4O6})]$ **(1)** deposited on mica substrates at different surface pressures for complex (b) layer thickness (nm) versus the number of lavers.

2r * h ≈ 272 Å2 (see **Figure S8**) This area is larger than the experimental average limiting area per molecule of ca. 185 $Å^2$, obtained from isothermal compression. The discrepancy suggests that each molecule shows a certain degree of overlap, yielding buckled or intercalated monolayers. This is also evidenced by transfer ratios between 1.1 and 1.3, thus slightly larger than expected (**Figure S11**).

Rectification behavior

The fabrication of Au|LB1|Au devices was necessary in order to test the rectification behavior of $[Fe^{III}_2(L^{N4O6})]$ (**1**). A PL monolayer was transferred from the air/water interface as an LB film onto a pre-cleaned gold substrate. The top gold electrode was gently deposited via gold sputtering using the shadow masking method on an Effa-Coater gold sputter. This method has yielded good results with our systems and has been described in detail elsewhere.[21, 22a] Five assemblies each containing 16 individual Au|LB1|Au devices were constructed, enabling current-voltage measurements of each device. About 6-8 devices per assembly were short-circuited due to defects on the monolayer. Rectification behavior was observed as asymmetric I-V curves with a sharp negative response and negligible positive response. The rectification ratio (*RR* = [I at $-V_o$/I at $+V_o$), an important parameter that characterizes the rectification behavior of a device,[49] varied from 2.6 to 9.8 between -2.0 and 2.0 V and between 4.5 and 15.5 between -4.0 and 4.0 V, as shown in **Figure 8** and **Figures S9-S10**. Retention of the rectification ratio was indicated by reversing the drain and the source contacts, which led the reversed current response expected for a diode-like molecule. Increased symmetry of the I-V curves was observed upon repeated measurements. This behavior has been observed for similar iron phenolate complexes and is attributed to reorientation of molecules to minimize dipole moment.[21, 22a, 36] Compared to other species in similar five-coordinate environments, the behavior of the Au|LB1|Au assembly is similar to that of monometallic $^{HS}Fe^{III}$ species in Au|LB|Au assemblies: Species $[Fe^{III}L^{N2O3}]^{21}$ showed RR values from 4.5 to 12 at ±2 V and from 3 to 37 at ±4 V, whereas $[Fe^{III}(L^{N2O2})Cl]^{22a}$ showed *RR* ranging from 4 to 29 at ±2 V and from 2 to 31 at ±4 V, thus comparable to the previous example. The latter species was also probed using EGaIn/Ga_2O_3|LB|Au assemblies[50] and yielded *RR* values of 3 and 12 at ±0.7 V and between 50 and 200 at ±1.0 V, with fast conversion to a sigmoidal curve after a few full scans. Using a similar EGaIn/Ga_2O_3|LB|Au assembly, a new species,[51] $[Fe^{III}(L^8)(OMe)_2]$ in which the ligand contains a pyridine and a phenolate, a maximum *RR* of 300 was observed between ±1 V. While the asymmetry of this species confirms the feasibility of rectification, a desired enhancement of the rectification ratio remains elusive. This is likely associated with the observed large average area per molecule that suggests limited film uniformity, where only certain molecules may contact the electrodes directly.

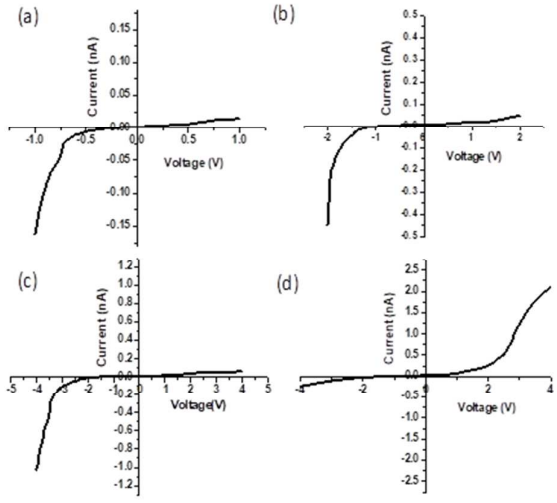

Figure 8: The I-V characteristics of $[Fe^{III}_2(L^{N4O6})]$ **(1)** obtained between (a) 1.0 and -1.0 V, (b) 2.0 and -2.0 V, and (c) 4.0 and -4.0 V. (d) shows the I-V curve obtained under reverse applied potential from 4.0 to -4.0 V.

Conclusions

In conclusion, we have successfully developed and studied an unprecedented bimetallic iron(III) hydrophobe described as $[Fe^{III}_2(L^{N4O6})]$ (**1**). The studies included synthesis, redox, spectroscopic and magnetic characterization, along with DFT calculations to simulate magnetic couplings. The CV of (**1**) suggests that the two metal centers are weakly coupled. This unique hydrophobe forms Pockels-Langmuir monolayers at the air-water interface showing a moderate collapse pressure of 32 mN/m. The associated Langmuir-Blodgett films were deposited onto glass substrates and films were investigated using IR-reflection/absorbance spectroscopy; the features of the film correlate well with those of the bulk IR spectrum of $[Fe^{III}_2(L^{N4O6})]$ indicating that the identity of the compound remains unchanged after deposition. Although some degree of overlap among the molecules was observed, assemblies were built in which LB monolayers sandwiched between two gold electrodes. Rectification of current was observed by asymmetric I-V curves. Based on previous arguments on the modulation of the frontier orbitals, we proposed that bimetallic systems may allow for inference on the role played by low molecular symmetry and orbital distortion. Considering the evidence for electronic coupling of the metal centers and facilitated SOMO-based electron transfer, the use of a C_{2v} molecule has clearly enabled current rectification. However, the large area measured per molecule observed by isothermal compression and by the scratching test suggests that only certain molecules display direct contact with the electrodes, thus precluding assessment of rectification enhancement. Ligand changes will be necessary in order to improve the amphiphilic behavior of such bimetallic species, and enable better film packing required for such assessment. These modifications are currently being pursued in our laboratories.

Experimental Section

Materials and methods

Reagents were used as purchased from commercial sources. A Varian 400 MHz instrument was used for ^{1}H-NMR spectra. Elemental analysis was performed by Midwest Microlab, Indianapolis, IN. Infrared spectrum of the complex was measured using a Tensor 27 FTIR-spectrophotometer in the range of 4000 to 600 cm^{-1} as KBr pellets. A Micromass LCT Premier XE (TOF) high resolution mass spectrophotometer was used to acquire the electrospray ionization (ESI) spectra. UV-visible spectra were collected using a Varian Cary 50 spectrophotometer in the range of 200-1100 nm. Cyclic voltammograms were obtained using a BAS 50W potentiostat. The standard three-electrode cell consisted of a glassy-carbon working electrode, a platinum-wire auxiliary electrode and an Ag/AgCl reference electrode. $TBAPF_6$ was used as supporting electrotrolyte and the ferrocene/ferrocenium redox couple Fc/Fc^+ ($E°$ = 400 mV vs. NHE) was used as the internal standard. [52]

Syntheses:

The ligand H_6L^{N4O6}. The ligand H_6L^{N4O6} was synthesized by the addition of 0.28 g of 1,2,4,5-benzenetetramine tetrahydrochloride (1.0 mmol) on to 1.52 g of 2,4-di-tert-butyl-6-(chloromethyl)phenol (6.0 mmol) and 2.1 mL of triethylamine (15 mmol) in dichloromethane. The resulting solution was heated under reflux for 24 h to complete the imine conversion. The reaction mixture was allowed to cool down to room temperature before being washed with brine solution. The organic layer was then dried over anhydrous sodium sulfate and rota-evaporated as a pale yellow powder. Yield: 1.0 g, 70 %). ^{1}H NMR, ppm ($CDCl_3$, 400 MHZ): δ 8.35 (s, 2H), δ 7.50- 8.36 (m, 14H), δ 4.10 (m, 8H), δ 3.88 (d, 2H), δ 1.07-1.44 (m, 54H). ESI (m/z) = 1449.1 for $[L + H^+]^+$.

The metal complex $[Fe^{III}_2(L^{N4O6})]$ (1). $[Fe^{III}_2(L^{N4O6})]$ was synthesized by dissolving 290 mg of L^{N4O6} (0.2 mmol) and 65 mg of sodium methoxide (1.2 mmol) in 20 mL of a 1:1 methanol:dichloromethane solution. To this solution 108 mg of $FeCl_3.6H_2O$ (0.4 mmol) dissolved in 5 mL of methanol were added dropwise. The resulting solution turned brown and was stirred for 3 h at 50 °C. The solution was subsequently filtered and X-ray quality crystals were obtained via slow evaporation from the mother liquor. Yield: 0.20 g (65 %). ESI-MS (m/z+; CH3OH) = 1550.8939, 100 % for $[C_{96}H_{132}N_4O_6Fe_2 + H^+]^+$. Anal. Calc. for $C_{96}H_{132}N_4O_6Fe_2$: 74.40; H: 8.59; N: 3.62; Found: C: 74.19; H: 8.94; N: 3.60.

Other physical methods:

X-ray structural characterization. Diffraction data were measured on a Bruker X8 APEX -II kappa geometry diffractometer with Mo radiation and a graphite monochromator. Frames were collected at 100K with the detector at 40 mm and 0.3 degrees between each frame and were recorded for 50 s. APEX-II[53] and SHELX[54] software were used for data collection and refinement of models. Crystals of $[Fe^{III}_2(L^{N4O6})]$ appeared as dark rhomboids and yielded a total of 160,610 reflections, from which 21,982 were unique (R_{int} =0.0664). Hydrogen atoms were placed at calculated positions. The solvate regions did not refine reasonably. The PLATON programme SQUEEZE[55]was utilized to account for the solvate electrons.

UV-visible spectroelectrochemistry. Spectroelectrochemical data was taken at room temperature using an optically transparent thin layer-cell, composed of a sandwich of two glass slides equipped with a U-shaped flat platinum working electrode that extended to the outside for electrical contact. The inner sides of the slides were coated with indium-tin oxide (ITO) (8-2 Ω/sq). A second platinum wire was used as a counter electrode and a pseudo Ag/AgCl wire served as the reference electrode. The $[Fe^{III}_2(L^{N4O6})]$ (**1**) species was dissolved in dichloromethane and purged with argon before being introduced into the cell through capillary interaction. Potentials of -1.35 and -1.70 $V_{Fc/Fc+}$ were applied to the cell for measurement of the reductive processes. The selected potentials assured that the respective reductions to $[Fe^{III}Fe^{II}(L^{N4O6})]$ and $[Fe^{II}_2(L^{N4O6})]$ occurred. These potentials were controlled using a BAS 50W potentiometer coupled to a Varian Cary 50 apparatus.

Electron paramagnetic resonance (EPR). Continuous wave (cw) X-band (9 - 10 GHz) EPR experiments of $[Fe^{III}_2(L^{N4O6})]$ (**1**) were carried out with an ELEXSYS II E500 EPR spectrometer from Bruker Biospin (Rheinstetten, Germany) equipped with a TE_{102} rectangular EPR resonator (Bruker ER 4102ST) and a helium gas-flow cryostat (ICE Oxford, UK). An intelligent temperature controller (ITC503) from Oxford Instruments, UK, was also used. Measurements on frozen solutions were done at cryogenic temperature (T = 30 K). Data processing was done using Xepr (Bruker BioSpin) and Matlab 7.11.2 (The MathWorks, Inc., Natick) environments.

Broken Symmetry Density Functional Theory (BS-DFT). Calculations were performed using the Gaussian 09 software package.[56] These calculations employed the B3LYP/6-311G functional/basis set combination, an unabridged X-ray based structural model, and a simplified geometry-optimized model for which all *tert*-butyl groups were replaced with H atoms. For the later models, geometry optimized structures were obtained for both the broken symmetry (BS) and the ferromagnetic (F) states. Geometry optimizations and single point, self-consistent field (SCF) calculations and were done using typical convergence criteria. The theoretical exchange coupling constants *J* were appraised by comparing the predicted SCF energies of the BS and F states.[57] The initial electronic points of the starting SCF calculations were obtained using the default guess option for the F configuration and the *fragment* option of the *guess* keyword for the BS states. For the homodinuclear $[Fe^{III}_2]$ complex the F state had an S_T = 5 configuration. The BS state corresponds to a S_T = 0 configuration for which 5α, spin-up, electrons are localized on

one iron site and 5β, spin-down, electrons were localized on the other iron site. The value of the exchange coupling constant was obtained using the expression $J=2(E_F-E_{BS})/25$ where the E_{BS} and E_F are the SCF energies obtained for the respective states. For the [$Cu^{II}Fe^{III}$] dimer the BS corresponds to a S_T = 2 and the F state S_T = 3 configuration. In this case, the coupling constant was obtained using the $J=2(E_F-E_{BS})/5$ expression. Charge and spin distributions were assessed based on the Mulliken atomic spin densities and charges.

Formation of Pockels-Langmuir and Langmuir-Blodgett films. The pressure vs. area (Π-A) isotherms of [$Fe^{III}_2(L^{N4O6})$] (**1**) were carried out using an automated KSV Minitrough (now Biolin, Espoo, Finland) at 22.8 ± 0.5 °C. Ultra-pure water with a resistivity of 17.5-18 MΩ.cm^{-1} was obtained from a Barnstead NANOpure system and used in all experiments. Impurities present at the surface of the freshly poured aqueous subphase were removed by vacuum after the compression of the barriers. Spreading solutions were prepared in spectra grade chloroform. A known quantity of [$Fe^{III}_2(L^{N4O6})$] (**1**) was dissolved in chloroform and 30 µL of a 1.0 mg/mL solution were spread over the water subphase. The system was allowed to equilibrate for approximately 20 min before monolayer compression. The Π vs. A isotherms were obtained at a compression rate of 10 mm.min^{-1}. The Wilhelmy plate method (paper plates, 20 × 10 mm) was used to measure the pressure.[58] At least three independent measurements were carried out per sample with excellent reproducibility attained. See **Figure S11**.

Brewster angle microscopy (BAM). A KSV-Optrel BAM 300 equipped with a HeNe laser (10mW, 632.8 nm) and a CCD detector was used in all micrographs of [$Fe^{III}_2(L^{N4O6})$] **(1)**. The compression rate was 10 mm/min, the field of view was 800 x 600 microns, and the lateral resolution was about 2-4 µm.

Infrared reflection absorption spectroscopy (IRRAS). Infrared reflection absorption spectroscopy of the LB films of [$Fe^{III}_2(L^{N4O6})$] **(1)** was carried out on a Bruker Tensor 27 infrared spectrophotometer outfitted with an A 513/Q variable-angle accessory, using s-polarization and an incidence angle of 30°. A 5-minute scanning time was used to obtain the IRRAS spectrum. The static contact angle of the modified substrates was determined at room temperature on a KSV CAM 200 goniometer equipped with a CCD camera.

Atomic force microscopy (AFM). Monolayers of LB films of [$Fe^{III}_2(L^{N4O6})$] **(1)** deposited at 17, 20, 25, and 30 mN.m^{-1} were probed in a Dimension 3100 AFM (VEECO) in the tapping mode in ambient air. The height, amplitude, and phase images were obtained using silicon tapping tips (nanoScience Instruments, VistaProbes T300) with resonance frequency of 300 kHz and a nominal tip radius less than 10 nm. The scan rate used was 0.5–2 Hz. Height images have been plane-fit in the fast scan direction with no additional filtering operation. Film thickness was determined by blade-scratching the film to expose the substrate, and then measuring the step height between the substrate and film surface at five different locations using the sectional height analysis.

Fabrication of Au|LB1|Au devices and measurement of I-V curves. Device fabrication used SPI supplied Au-coated mica substrates covered with LB films of [$Fe^{III}_2(L^{N4O6})$] **(1)** at 25 mN/m. The top Au-electrode was coated on an EffaCoater gold sputter using the shadow masking method. The current–voltage (*I-V*) characteristics of the devices were measured using a Keithley 4200 semiconductor parameter analyzer coupled to a Signatone S-1160 Probe Station at ambient conditions.

Conflicts of interest

There are no conflicts to declare.

Acknowledgements

The authors thankfully acknowledge support from the National Science Foundation through the grants NSF-CHE1012413 and NSF-CHE-1500201 to CNV, including partial financial support to ADKIW and HB, as well as to the U.S. Department of Energy, Office of Science, Office of Basic Energy Sciences, under contract number DE-AC02-06CH11357 at Argonne National Laboratory to JN and OP. SAS acknowledges the support from the University of Idaho and HB acknowledges the WSU-Department of Chemistry for a Thomas C. Rumble Graduate Fellowship.

Notes and references

1 A. Aviram and M. A. Ratner, Chem. Phys. Lett., 1974, **29**, 277-283.
2 (a) R. M. Metzger, Chem. Rev., 2003, **103**, 3803-3834; (b) R. M. Metzger, Chem. Rev. 2015, **115**, 5056-5115.
3 G. J. Ashwell and D. S. Gandolfo, J. Mater. Chem., 2001, **11**, 246-248.
4 L. D. Wickramasinghe, S. Mazumder, K. K. Kpogo, R. J. Staples, H. B. Schlegel and C. N. Verani, Chem. – A Eur. J., 2016, **22**, 10786-10790.
5 S. V. Aradhya and L. Venkataraman, Nat. Nanotech., 2013, **8**, 399.
6 A. Honciuc, A. Otsuka, Y.-H. Wang, S. K. McElwee, S. A. Woski, G. Saito and R. M. Metzger, J. Phys. Chem. B, 2006, **110**, 15085-15093.
7 C. Krzeminski, C. Delerue, G. Allan, D. Vuillaume and R. M. Metzger, Phys. Rev. B, 2001, **64**, 085405.
8 R. M. Metzger, Acc. Chem. Res., 1999, **32**, 950-957.
9 R. M. Metzger, Chem. Rec., 2004, **4**, 291-304.
10 R. M. Metzger, J. Mater. Chem., 2008, **18**, 4364-4396.
11 R. M. Metzger, Nanoscale, 2018, **10**, 10316-10332.
12 J. Hyunhak, K. Dongku, W. Gunuk, P. Sungjun, L. Hanki, C. Kyungjune, H. Wang-Taek, Y. Myung-Han, J. Y. Hee, S. Hyunwook, X. Dong and L. Takhee, Adv. Funct. Mater., 2014, **24**, 2472-2480.

13 J. Jiang, J. A. Spies, J. R. Swierk, A. J. Matula, K. P. Regan, N. Romano, B. J. Brennan, R. H. Crabtree, V. S. Batista, C. A. Schmuttenmaer and G. W. Brudvig, J. Phys. Chem. C, 2018, **122**, 13529-13539.
14 Y. Lee, S. Yuan, A. Sanchez and L. Yu, Chem. Commun., 2008, DOI: 10.1039/B712978E, 247-249.
15 E. D. Mentovich, N. Rosenberg-Shraga, I. Kalifa, M. Gozin, V. Mujica, T. Hansen and S. Richter, J. Phys. Chem. C, 2013, **117**, 8468-8474.
16 H. Murni, G. Syun, T. Daisuke and O. Takuji, Chem. – A Eur. J., 2014, **20**, 7655-7664.
17 E. A. Osorio, K. Moth-Poulsen, H. S. J. van der Zant, J. Paaske, P. Hedegård, K. Flensberg, J. Bendix and T. Bjørnholm, Nano Lett., 2010, **10**, 105-110.
18 W. J. Pietro, Adv. Mater., 1994, **6**, 239-242.
19 M. A. Sierra, D. Sanchez, A. R. Garrigues, E. del Barco, L. Wang and C. A. Nijhuis, Nanoscale, 2018, **10**, 3904-3910.
20 S. Sun, X. Zhuang, L. Wang, B. Zhang, J. Ding, F. Zhang and Y. Chen, J. Mater. Chem. C, 2017, **5**, 2223-2229.
21 L. D. Wickramasinghe, M. M. Perera, L. Li, G. Mao, Z. Zhou and C. N. Verani, Angew. Chem. Int. Ed., 2013, **52**, 13346-13350.
22 (a) L. D. Wickramasinghe, S. Mazumder, S. Gonawala, M. M. Perera, H. Baydoun, B. Thapa, L. Li, L. Xie, G. Mao, Z. Zhou, H. B. Schlegel and C. N. Verani, Angew. Chem. Int. Ed., 2014, **53**, 14462-14467; (b) C. A. Nijhuis, W. F. Reus, and G. M. Whitesides J. Am. Chem. Soc. 2010, **132**, 18386–18401. (c) P.E. Kornilovitch, A.M. Bratkovsky, and R. Stanley Williams Physical Review B 2002, **66**, 165436.
23 M. M. Allard, J. A. Sonk, M. J. Heeg, B. R. McGarvey, H. B. Schlegel and C. N. Verani, Angew. Chem. Int. Ed., 2012, **51**, 3178-3182.
24 M. Lanznaster, M. J. Heeg, G. T. Yee, B. R. McGarvey and C. N. Verani, Inorg. Chem., 2007, **46**, 72-78.
25 The tau index is $\tau = (\beta - \alpha)/60$, where β is the largest and α is the second largest angles in the coordination sphere as described by A. W. Addison, T. N. Rao, J. Reedijk, J. van Rijn and G. C. Verschoor, Dalton Trans., 1984, **5**, 1349-1356.
26 K. S. Min, A. L. Rheingold, A. DiPasquale and J. S. Miller, Inorg. Chem., 2006, **45**, 6135-6137.
27 J. A. DeGayner, I.-R. Jeon and T. D. Harris, Chem. Sci., 2015, **6**, 6639-6648.
28 S. W. Gordon-Wylie, B. L. Claus, C. P. Horwitz, Y. Leychkis, J. M. Workman, A. J. Marzec, G. R. Clark, C. E. F. Rickard, B. J. Conklin, S. Sellers, G. T. Yee and T. J. Collins, Chem. – A Eur. J., 1998, **4**, 2173-2181.
29 A. Aukauloo, X. Ottenwaelder, R. Ruiz, S. Poussereau, Y. Pei, Y. Journaux, P. Fleurat, F. Volatron, B. Cervera and M. C. Muñoz, Eur. J. Inorg. Chem., 1999, **1999**, 1067-1071.
30 M. B. Robin and P. Day, in Advances in Inorganic Chemistry and Radiochemistry, eds. H. J. Emeléus and A. G. Sharpe, Academic Press, 1968, vol. 10, pp. 247-422.
31 M. H. Chisholm and N. J. Patmore, Acc. Chem. Res., 2007, **40**, 19-27.
32 D. E. Richardson and H. Taube, Determination of E2° - E1° in multistep charge transfer by stationary-electrode pulse and cyclic voltammetry: Application to binuclear ruthenium ammines, 1981.
33 M. Glöckle and W. Kaim, Angew. Chemi. Int. Ed., 1999, **38**, 3072-3074.
34 M. M. Allard, F. R. Xavier, M. J. Heeg, H. B. Schlegel and C. N. Verani, Eur. J. Inorg. Chem., 2012, DOI: 10.1002/ejic.201200171, 4622-4631.
35 M. M. Allard, J. A. Sonk, M. J. Heeg, B. R. McGarvey, H. B. Schlegel and C. N. Verani, Angew. Chem. Int. Ed., 2012, **51**, 3178-3182.
36 I. Brand, J. Juhaniewicz-Debinska, L. Wickramasinghe and C. N. Verani, Dalton Trans., 2018, DOI: 10.1039/C8DT00333E.
37 K. Kitagawa, T. Morita and S. Kimura, Langmuir, 2005, **21**, 10624-10631.
38 K. Seo, A. V. Konchenko, J. Lee, G. S. Bang and H. Lee, J. Am Chem. Soc., 2008, **130**, 2553-2559.
39 M. S. Johnson, L. Wickramasinghe, C. Verani and R. M. Metzger, J. Phys. Chem. C, 2016, **120**, 10578-10583.
40 F. D. Lesh, R. Shanmugam, M. M. Allard, M. Lanznaster, M. J. Heeg, M. T. Rodgers, J. M. Shearer and C. N. Verani, Inorg. Chem., 2010, **49**, 7226-7228.
41 K. B. Blodgett, J. Am. Chem. Soc., 1934, **56**, 495-495.
42 K. B. Blodgett, J. Am. Chem. Soc., 1935, **57**, 1007-1022.
43 I. Langmuir, J. Am. Chem. Soc., 1917, **39**, 1848-1906.
44 G. Roberts, in Langmuir-Blodgett Films, Springer, 1990, pp. 317-411.
45 S. Kundu, A. Datta and S. Hazra, Langmuir, 2005, **21**, 5894-5900.
46 S. Kundu, A. Datta and S. Hazra, Phys. Rev. E, 2006, **73**, 051608.
47 T. Leitner, J. Kattner and H. Hoffmann, *Appl. Spectrosc.*, 2003, **57**, 1502-1509.
48 H. H. J. Kattner, *External reflection spectroscopy of thin films on dielectric substrates: Handbook of vibrational spectroscopy*, John Wiley & Sons Ltd., Chichester, 2002.
49 R. M. Metzger, B. Chen, U. Höpfner, M. V. Lakshmikantham, D. Vuillaume, T. Kawai, X. Wu, H. Tachibana, T. V. Hughes, H. Sakurai, J. W. Baldwin, C. Hosch, M. P. Cava, L. Brehmer and G. J. Ashwell, *J. Am. Chem. Soc.*, 1997, **119**, 10455-10466.
50 M. S. Johnson, L. Wickramasinghe, C. Verani and R. M. Metzger, *J. Phys. Chem. C*, 2016, **120**, 10578-10583.
51 M. S. Johnson, C. L. Horton, S. Gonawala, C. N. Verani and R. M. Metzger, *Dalton Trans.*, 2018, **47**, 6344-6350.
52 (a) N. G. Connelly and W. E. Geiger, *Chem. Rev.*, 1996, **96**, 877-910 (b) R. R. Gagne, C. A. Koval and G. C. Lisensky, *Inorg. Chem.*, 1980, **19**, 2854-2855.
53 M. Bruker AXS Inc., WI, USA, *Journal*, 2009.
54 G. M. Sheldrick, *Acta Crystallogr. Sect. A*, 2008, **64**, 112-122.
55 A. L.. Spek, *J. Appl. Crystallogr.*, 2003, **36**, 7-13.
56 M. J. Frisch, G. W. Trucks, H. B. Schlegel, G. E. Scuseria, M. A. Robb, J. R. Cheeseman, G. Scalmani, V. Barone, B. Mennucci, G. A. Petersson, H. Nakatsuji, M. Caricato, X. Li, H. P. Hratchian, A. F. Izmaylov, J. Bloino, G. Zheng, J. L. Sonnenberg, M. Hada, M. Ehara, K. Toyota, R. Fukuda, J. Hasegawa, M. Ishida, T. Nakajima, Y. Honda, O. Kitao, H. Nakai, T. Vreven, J. A. Montgomery, Jr., J. E. Peralta, F. Ogliaro, M. Bearpark, J. J. Heyd, E. Brothers, K. N. Kudin, V. N. Staroverov, T. Keith, R. Kobayashi, J. Normand, K. Raghavachari, A. Rendell, J. C. Burant, S. S. Iyengar, J. Tomasi, M. Cossi, N. Rega, J. M. Millam, M. Klene, J. E. Knox, J. B. Cross, V. Bakken, C. Adamo, J. Jaramillo, R. Gomperts, R. E. Stratmann, O. Yazyev, A. J. Austin, R. Cammi, C. Pomelli, J. W. Ochterski, R. L. Martin, K. Morokuma, V. G. Zakrzewski, G. A. Voth, P. Salvador, J. J. Dannenberg, S. Dapprich, A. D. Daniels, O. Farkas, J. B. Foresman, J. V. Ortiz, J. Cioslowski, and D. J. Fox, Gaussian 09 (Revision D.01) Gaussian, Inc., Wallingford CT, 2013.
57 L. Noodleman and E. J. Baerends, *J. Am. Chem. Soc.*, 1984, **106**, 2316-2327.
58 A. Gopal, V. A. Belyi, H. Diamant, T. A. Witten and K. Y. C. Lee, Los Alamos Natl. Lab., Prepr. Arch., Condens. Matter 2004, arXiv:condmat/0409147.